Check for updates

Alkanes as Intelligent Surface Thermometers: A Facile Approach to Characterize Short-Lived Temperature Gradients on the Micrometer Scale

Stephan Eickelmann,* Sebastian Ronneberger, Junfang Zhang, Grigori Paris, and Felix F. Loeffler*

Short-lived micro-sized thermal gradients are challenging to measure. Especially, in thin film processes and devices, it is important to know the exact temperature profile to assure process parameters and the stability of sensitive materials. Many theoretical models try to describe the occurring temperatures, but still lack in profound experimental data. Here, a facile approach is presented, which allows to measure confined temperature gradients with millisecond and micrometer precision. By casting a thin alkane film onto a substrate of interest, it is possible to reconstruct local temperature gradients by imaging the phase behavior and morphology of the alkane film with a simple optical microscope setup. Alkanes are inert and their melting and boiling temperatures depend on the chain length. This allows to measure temperatures between 37 and 522 °C on any surface. Furthermore, after thorough characterization of laser-induced temperature gradients, this approach can be used to measure the phase transition behavior of complex thin film polymer mixtures.

1. Introduction

A major challenge in science and technology is the control and measurement of rapidly changing, spatially, and temporally confined temperature gradients. The smaller and thinner a system becomes, the more problematic is the heat management, for example, in batteries,[1] solar cells,[2] and semiconductor components.[3] With progressive miniaturization, it becomes increasingly difficult to find non-invasive methods for the characterization of short-lived thermal gradients.

One of the most common techniques to generate local temperature gradients is through laser irradiation. Laser material

processing and probing have become universal standard techniques in research and industry. This extends from engineering applications, such as laser cutting, welding, and surface treatment,[4] bio-medical applications, such as eye surgery,[5] to applications in materials science and chemistry,[6,7] to assist in the synthesis of colloids,[8] nanoparticles,[9] and graphene.[10,11]

In recent years, the manipulation of thin films with lasers has gained a lot of attention: Laser-induced forward transfer (LIFT)[12] utilizes a laser to transfer materials from a donor thin film to an acceptor surface to create patterns. Thereby, sensitive biomolecules can be transferred inside a carrier (solvents or polymers) to generate microarrays.[13–17]

Focused laser irradiation can easily introduce a thermal gradient into a complex thin film system on the micrometer scale. However, it is critical to control the exact conditions during processing to assure stability of sensitive materials. Many numerical and theoretical models[18] try to describe the occurring temperatures in single material films. Yet, profound experimental data of such small and short-lived temperature gradients in complex thin films is scarce.

Current technologies for thermal microscale measurements[19,20] comprise for example of thermal reflectance methods,[21–23] micro-sized thermal probes,[24] thermal mapping with nematic liquid crystals,[25,26] fluorescence,[27] and infrared measurements.[28] These approaches are too slow, do not offer sufficient lateral resolution, and can only be addressed by expensive and complicated setups. In addition, some of these techniques cause major perturbations (e.g., altering the heat capacity) in the rapidly changing ultrathin film systems (μm to nm range), making precise measurements impossible.

In this work, we introduce a facile methodology to measure spatially and temporally confined surface temperature gradients with micrometer and millisecond precision. By casting a thin alkane film onto a planar substrate of interest, we can simply image a local laser-induced temperature gradient, due to the change of morphological properties of the alkane film. These nanometer thin structures can easily be imaged with standard optical microscopy techniques.[29,30] Alkanes are inert, non-conductive, transparent, and well characterized. Their temperature

Dr. S. Eickelmann, S. Ronneberger, J. Zhang, G. Paris, Dr. F. F. Loeffler
Max-Planck-Institute of Colloids and Interfaces
Biomolecular Systems
Am Muehlenberg 1, Potsdam 14476, Germany
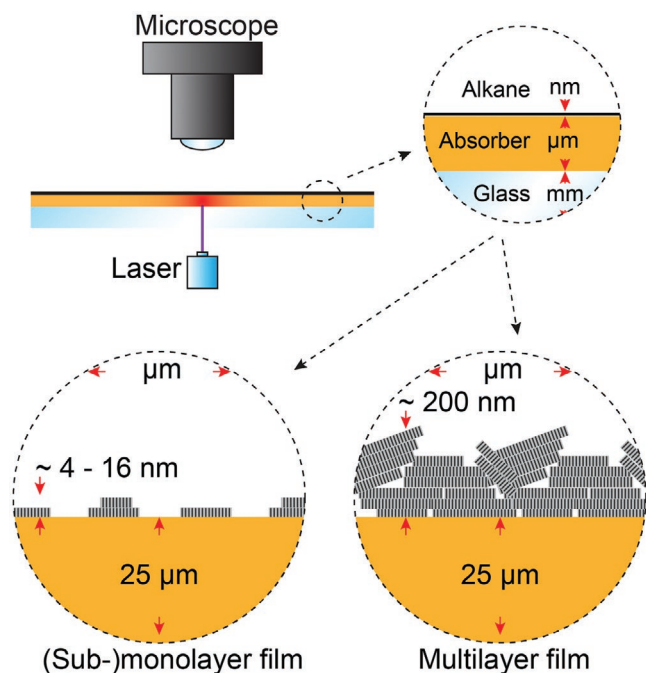E-mail: stephan.eickelmann@mpikg.mpg.de; felix.loeffler@mpikg.mpg.de

Figure 1. Basic setup for time resolved microscopy of the process. Typical samples are (sub-)mono to multilayer alkane films, coated onto a laser absorber (25 µm thick polyimide) film, supported by a standard 1 mm microscope glass slide.

behavior, as well as, their melting and boiling points (here, 37–522 °C) depend on their chain length.[30–34]

The basic setup (**Figure 1**) consists of a standard glass slide, supporting a thin film laser absorber. In particular, we used a polyimide film of 25 µm thickness. A laser is focused onto the film from underneath (spot size $d_{spot} = 40$ µm, see Figure S1, Supporting Information). Since the polyimide is coated with a (sub-)mono or multilayer of alkanes, a simple reflective optical microscope setup[29] is used to image the thin film. We used a fast high-resolution camera with 1000 fps, which is not required but useful for in situ imaging.

After thorough characterization of different short-lived laser-induced temperature gradients, this approach can be used to measure the phase transition behavior of complex thin film polymer mixtures.

2. Results

2.1. Melting and Time Evolution of Alkane Films under Laser-Induced Heating

In **Figure 2**, we show the behavior of a multilayer alkane coating during irradiation of the supporting 25 µm polyimide film. The schematic illustrates the morphology and phase evolution of the alkane crystal structures. Directly after the first melt appears, the film starts to rupture and a de-wetting rim forms, which follows the melting perimeter (ring) during the process.

Some small alkane droplets remain on the surface in the rupture hole. These droplets start to disappear after a certain time, which can be correlated to the evaporation of these droplets, since the surface center reaches the boiling point of the alkane.
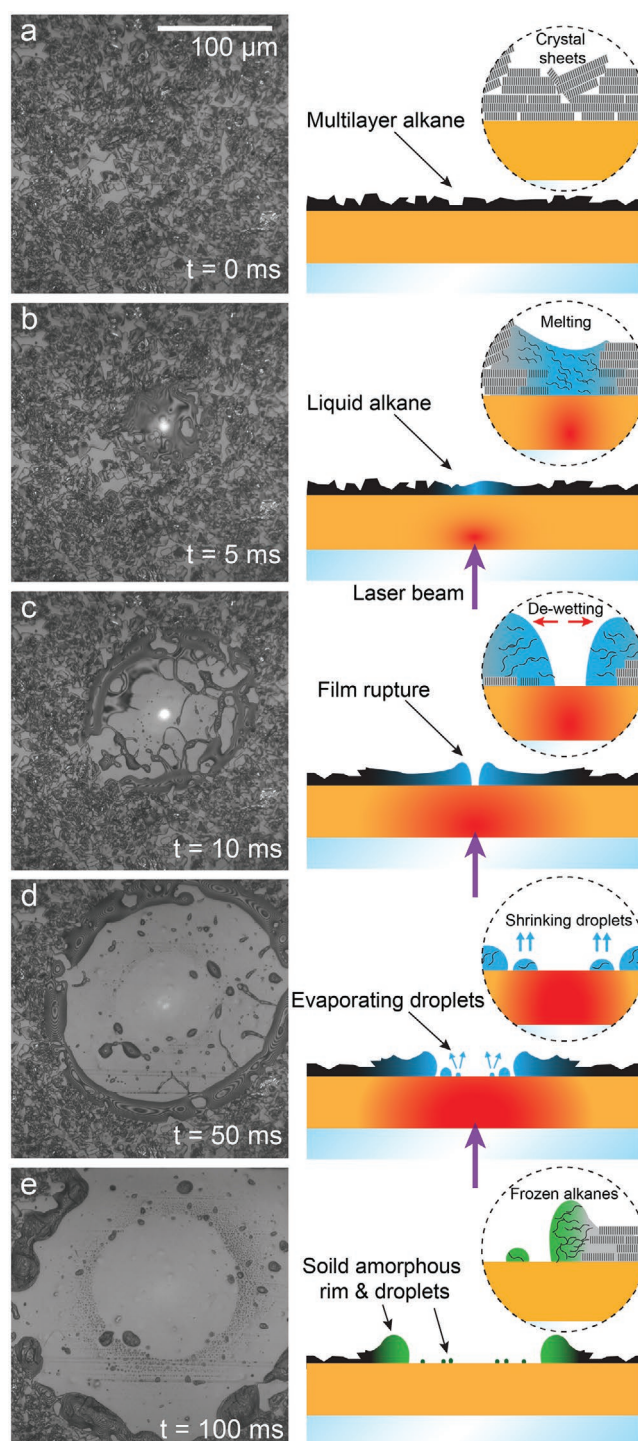

Figure 2. Time evolution of alkane melting during laser irradiation: a) The solid alkane multilayer film, b) initial melting due to laser irradiation, c) melting and rupture of film and ring formation. d) Evaporation of tiny residual alkane droplets. e) Rapidly solidified amorphous alkane de-wetting rim.

Additionally, tiny droplets appear between the perimeters of melting and evaporation, presumably as a result of condensation of gaseous alkanes at the slightly colder surface. These droplets disappear again when the evaporation perimeter further expands.
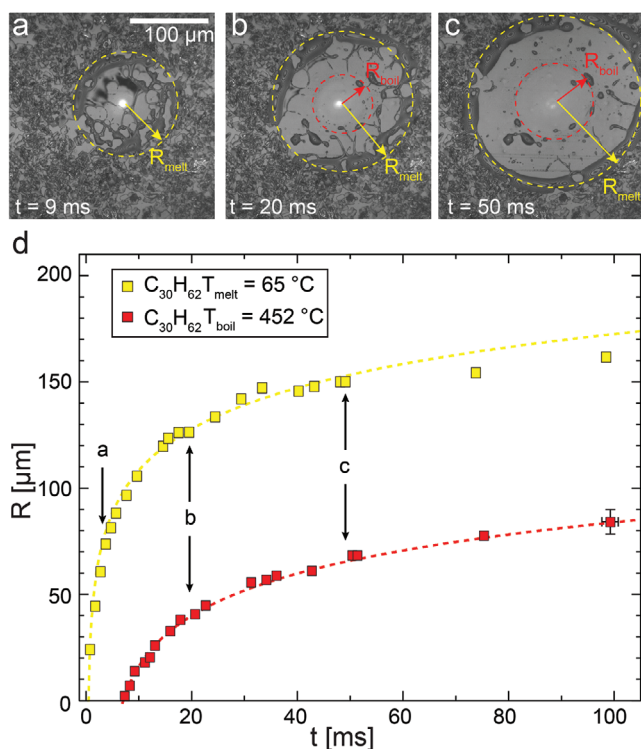
Figure 3. Image sequence for a 50 mW laser irradiation on a $C_{30}H_{62}$ multilayer film. a) Shortly after the beginning of laser irradiation, the liquid alkane forms a rupture hole (R_{melt}), while a fine layer of small alkane droplets remains on the surface. b) The rupture hole grows over time and a second (inner) ring (R_{boil}) forms at the boundary of the fine droplet layer and the dry surface. c) Both perimeters continue to grow. d) Radial measurements of the melting and evaporation perimeter. Error bars are omitted to improve visualization; a representative error bar is shown in the graph (bottom right).

From the microscopy data, we measure the radial increase of the rupture hole and the perimeter of the disappearing small droplets. **Figure 3** shows an image sequence with the radii of the melting and boiling rings. From these results, following the growth of these rings, we can derive radial isothermal data points for the melting and boiling temperature of the alkane (Figure 3d, see Figure S11 (Supporting Information) for details on the measurement and errors).

2.1.1. Comparison of Rupture and Wetting Effects with the Melting Perimeter

To avoid that rupture and wetting effects conceal the melting perimeter, as well as to analyze the influence of the material thickness on heat capacity, we additionally prepared ultrathin sub-monolayers (<4–16 nm) and very thick multilayer (>−200 nm) coatings of alkanes on the polyimide surface.

We compared the melting/boiling behavior of a sub-monolayer (**Figure 4**a) against a multilayer (Figure 4b) $C_{36}H_{74}$ under identical irradiation conditions. The evolution of the melting perimeter (single droplets appearing and crystal structures disappearing) and boiling perimeter (single droplets disappearing) show that the radii of both experiments match within measurement error. While the thick layer behaves

as already described, the sub-monolayer coating shows no macroscopic de-wetting effects, because the molten alkane droplets are too far away from each other to merge. Thus, only the transition from alkane crystal structures to liquid droplets is visible, without movement on the surface. The boiling perimeters behave similarly, both showing the condensation ring.

Based on this observation and the fact that both coatings are thin in comparison to the laser absorbing polyimide layer, we can neglect the influence of the heat capacity of the alkane layer. Thus, the melting and boiling events should directly correlate with the temperature on the polyimide surface.

2.1.2. Radial Isotherms for Alkanes of Different Chain Lengths

Next, we analyzed the radial expansion, deriving isotherms at different irradiation conditions (**Figure 5**a) and different temperatures (Figure 5b).

We display the melting isotherms for $C_{36}H_{74}$ at 76 °C with respect to the laser intensity (Figure 5a). Upon the highest irradiation power, the isotherm grows the fastest, while at lower power the overall expansion stays smaller.

A list, comprising all used alkanes with their corresponding melting and boiling temperatures can be found in Table S1 in the Supporting Information.

Now, considering only the 100 mW laser power (Figure 5b), we display the isotherms for different temperatures. The $C_{20}H_{42}$ alkane (melting temperature of 37 °C) shows the biggest expansion radius, while with increasing temperature, the expansion eventually plateaus.

All isotherms were fitted with a simple logarithmic function to create a guide to the eye and an extrapolation of intermediate values (see the Supporting Information). For longer irradiation times, the logarithmic fit deviates from the data, but it agrees well with the initial part of the process.

2.2. Spatial and Temporal Reconstruction of Thermal Gradients from Alkane Measurements

From the previous measurements, we now extract the concurrently appearing characteristic melting and boiling radii from the isotherms shown in Figure 5 and reconstruct spatial temperature profiles for various times (shown in **Figure 6**a).

Data points were fitted with a Gaussian (see the Supporting Information), which allows us to extrapolate temperature values in between the mapped values. Temperatures higher than 522 °C can only be estimated.

By employing our previously obtained knowledge, we can now perform an offline measurement: First, we irradiate the surface with different laser powers and various irradiation times, creating a pattern of different wetting and evaporation rings (shown in Figure S2 in the Supporting Information). Immediately after the irradiation stops, the process stops and the alkane freezes in place, conserving the history of the melting and boiling process.

Then, we can image the (static) surface and overlay our previous profiles to reconstruct a snapshot of the spatial temperature gradients (Figure 6b,c).

The melting temperature of $C_{30}H_{62}$ (65 °C) agrees with the melt and rupturing radius in Figure 6b and a secondary

ADVANCED
SCIENCE NEWS
www.advancedsciencenews.com

ADVANCED
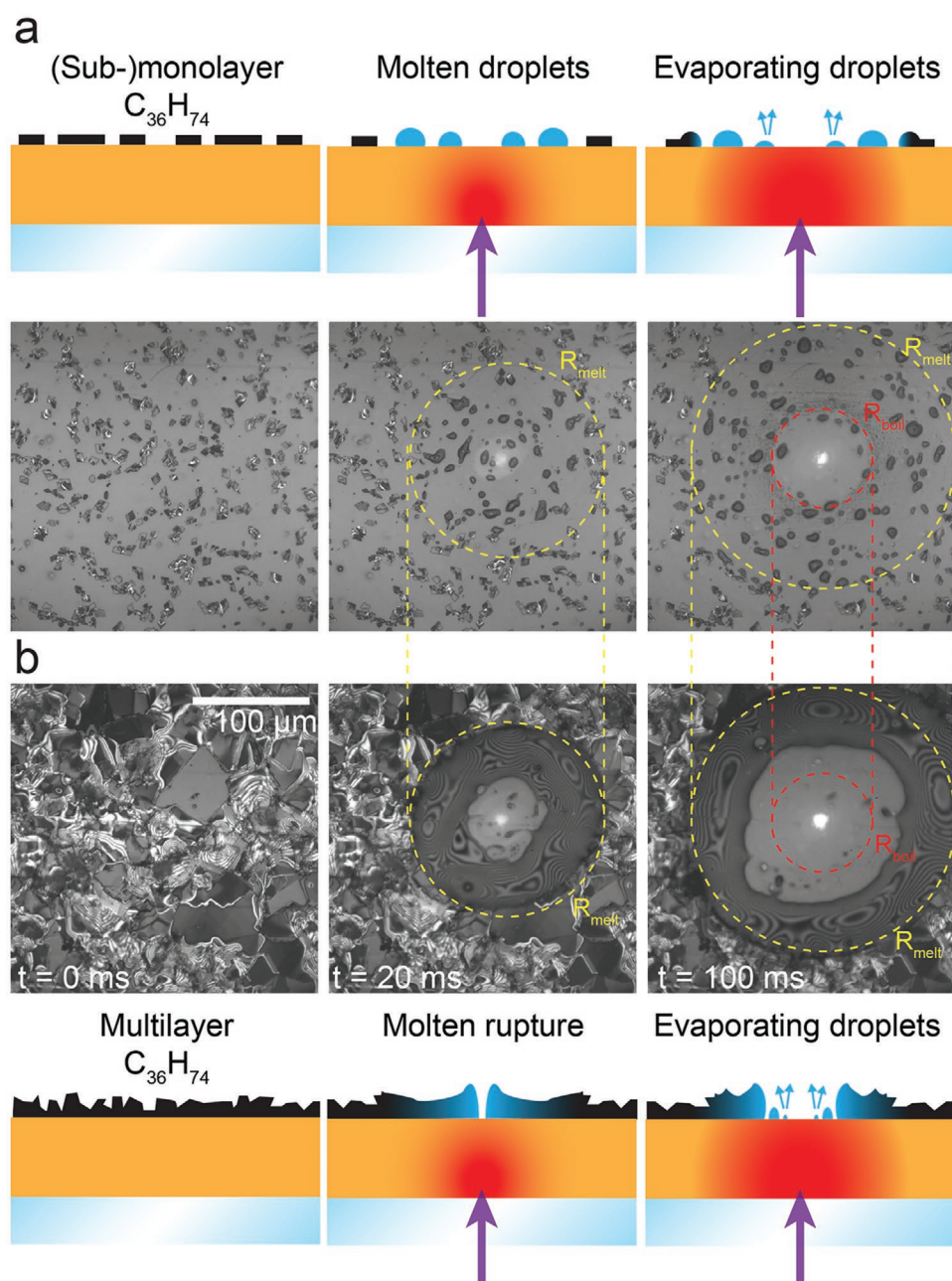**MATERIALS**
INTERFACES
www.advmatinterfaces.de

Figure 4. Melting of $C_{36}H_{74}$ alkane (sub-)monolayer a) versus multilayer b): The heat capacity of the alkane coating can be neglected, since no significant differences in the extent of the melting perimeters can be observed,

radius for the boiling temperature (452 °C) agrees with a perimeter formed by the transition from small droplets to a dry surface.

To verify our approach, a thin coating of $AgNO_3$ silver nitrate on the polyimide surface was heated with the laser. The melting point of silver nitrate is known to be $T_m = 212$ °C.[35]

Overlaying the corresponding thermal profile with the microscopic image taken after 10 ms with 100 mW laser irradiation (Figure 6c) results in an extracted surface temperature of around 213 ± 5 °C at the melting perimeter of the coating.

2.3. Determining the Critical Phase Change Temperature of Complex Systems

In a more sophisticated approach, instead of using an alkane, we now mixed a polystyrene acrylic copolymer (SLEC PLT 7552, Sekisui Chemical GmbH, Düsseldorf/Nordrhein-Westfalen, Germany) with 10% w/w amino acid building blocks (e.g., alanine) and coated polyimide films with these mixtures.[15,17] The thickness of these polymer mixture films is around 180 nm and they form closed homogenous films with slight surface roughness. Upon laser irradiation, the polymer reaches a critical
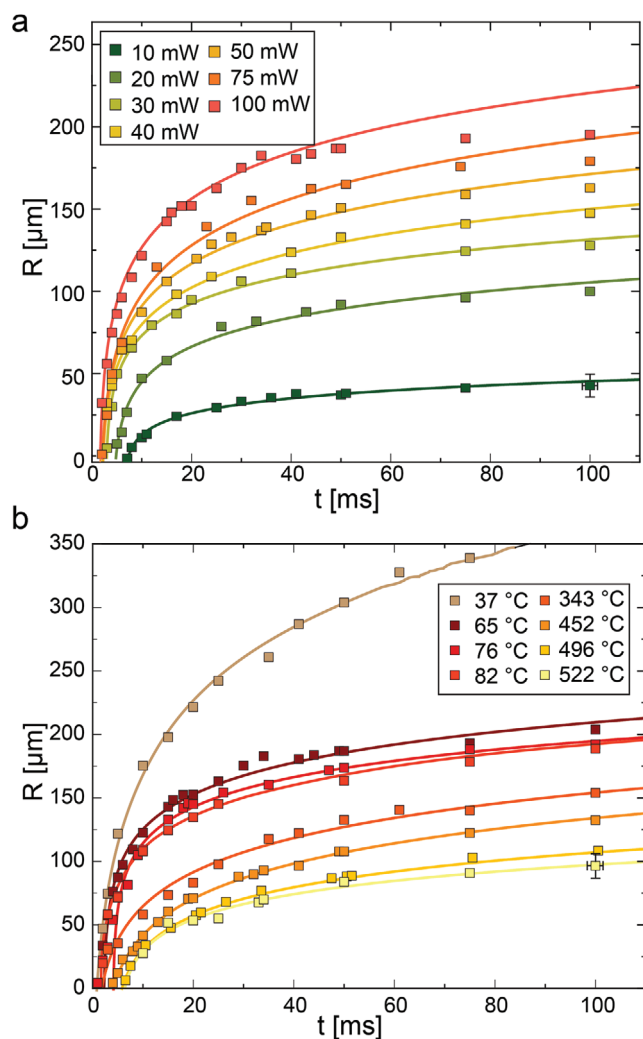
**ADVANCED
SCIENCE NEWS**

www.advancedsciencenews.com

**ADVANCED
MATERIALS
INTERFACES**

www.advmatinterfaces.de

Figure 5. a) Isotherms of 76 °C at different laser powers for the melting of $C_{36}H_{74}$. b) Isotherms for different melting and boiling temperatures for constant 100 mW laser irradiation. Solid lines represent logarithmic fit of the corresponding data. Error bars are omitted to improve visualization; a representative error bar is shown in the graphs (bottom right).

temperature T_{crit}, where conformational and structural changes occur (glass transition or melting). The changes expand radially around the laser spot. In contrast to the multilayer alkane films, no de-wetting or rupture can be observed (see Figure S7, Supporting Information).

From the measurements, we extract the radial expansion of the melting perimeter. After plotting this data over time, we find a similar behavior as for the alkane systems (Figure S7b, Supporting Information). In this case, the specific critical temperature and exact behavior of these polymer mixtures is unknown.

By utilizing our knowledge on the precise surface temperature of the polyimide and assuming that the polymer mixture is thin enough in comparison to the supporting polyimide film (i.e., negligible heat capacity), we can reconstruct the critical temperature T_{crit}, where conformational and structural changes of the complex polymer mixture occur.
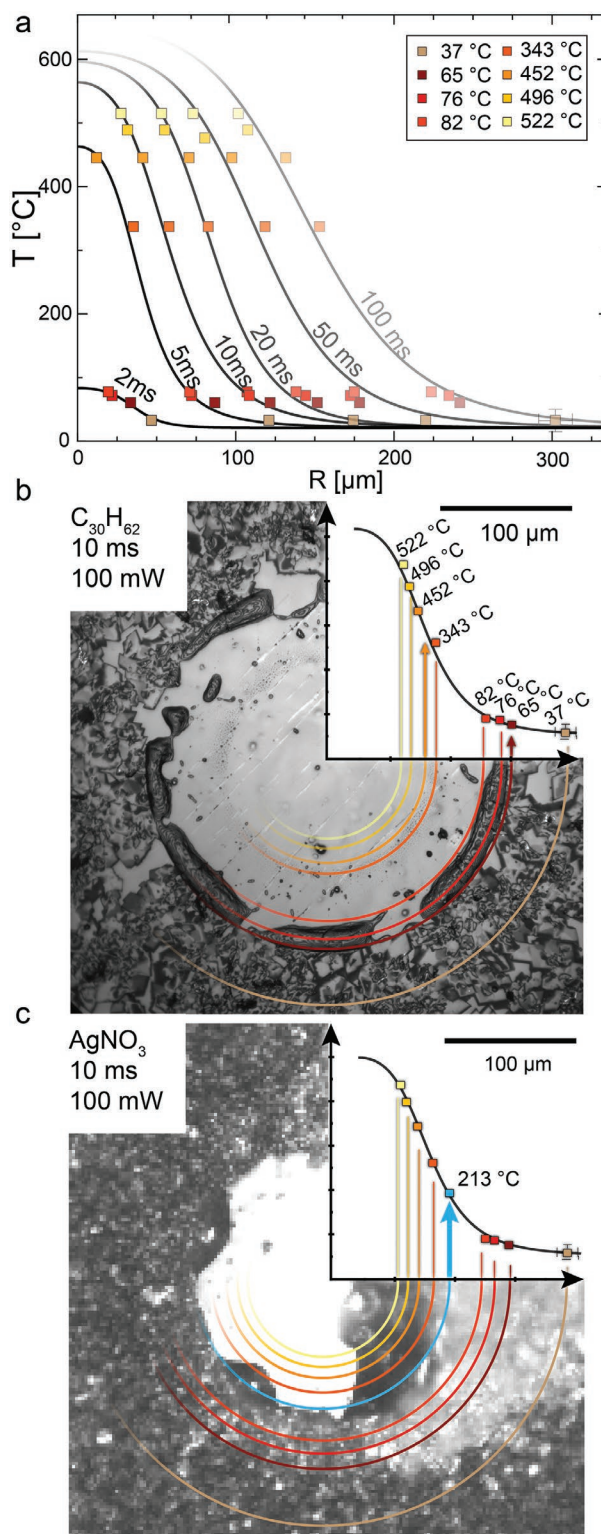

Figure 6. a) Reconstructed thermal profiles during the irradiation at 100 mW laser power, b) thermal map of a 10 ms laser irradiation of the polyimide coated with a thin $C_{30}H_{62}$ film and c) temperature overlay of an $AgNO_3$ coated surface, irradiated under the same conditions. The blue line indicates correlation of the melting perimeter to the apparent surface temperature. Error bars are omitted to improve visualization; a representative error bar is shown in the graphs (bottom right).
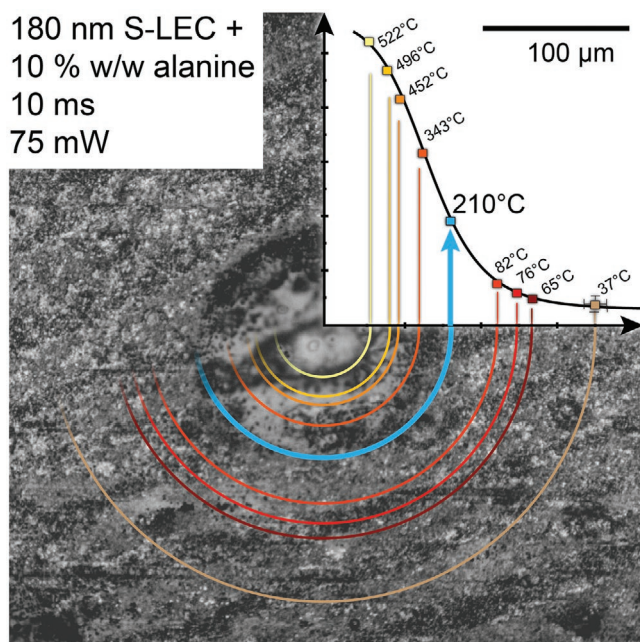
**ADVANCED
SCIENCE NEWS**
www.advancedsciencenews.com

**ADVANCED
MATERIALS
INTERFACES**
www.advmatinterfaces.de

Figure 7. Microscopic image of a polymer mixture, irradiated at 75 mW power for 10 ms. Colored rings represent the overlay of isotherms from corresponding alkane measurements with reference to the profiles plotted in the inset. The melting radius of the polymer (blue line) corresponds to surface temperature of 210 °C. Error bars are omitted to improve visualization; a representative error bar is shown in the graph (bottom right).

We demonstrate such a measurement for a mixture of polystyrene acrylic copolymer with 10% w/w alanine with the already mapped laser power of 75 mW. **Figure 7** shows the temperature profiles extracted from the alkane isotherms and compares the isothermal measurement to the polymer mixture. We easily correlate the corresponding melting radii with the temperature profile extracted from the alkane measurements.

For this specific polymer mixture, we determined a critical temperature of T_{crit} of 210 °C on the basis of the optically visible "melting" perimeter. The reported glass transition temperature T_g for these polymer mixtures is between 70–80 °C,[36] thus, we apparently observe a different phase transition, which likely correlates with melting.

Repeating this procedure for several time points during the irradiation (shown in Figure S8, Supporting Information), we found that the melting radii for different polymer mixtures always correspond to the same critical temperature value of T_{crit} of 210 ± 5 °C within measurement error.

3. Discussion and Conclusion

For many thin film processes, the exact measurement of spatially and temporally confined thermal gradients is important. However, current thermal measurement technologies are either impractical or too slow. Using alkanes as thermal reporters offers a cheap alternative. Since the thickness of the alkane film can easily be tuned in the nanometer range via spin casting (even sub-monolayers can be used), the heat capacity of the

alkane can be neglected and the behavior of the alkane directly reflects the induced surface temperature. In contrast, thermal measurements with liquid crystal always require a closed layer. This drastically changes the surface properties (e.g., conductivity) and hampers the precise measurement of temperature gradients generated by electric arcs and ion beams.

Using different alkanes, temperatures between 37 and 522 °C can be mapped by analyzing the footprint of the melting and boiling perimeters. As soon as the heat source is switched off, the alkane layer conserves the maximum gradient by solidifying in its final state. Additionally, the history of the solidification is preserved in the alkane structure, as they organize to different structures based on the solidification mechanism, which can be optically distinguished (Figure S9, Supporting Information).[30,33,34] For short-lived temperature gradients, they follow a logarithmic behavior (Figure 5 and Figures S3 and S6: Supporting Information).

While we followed the processes in situ with a more expensive camera setup, it is sufficient to create snapshots of temperature gradients with increasing energy to reconstruct the evolution of a thermal profile (Figure S2, Supporting Information).

Our approach is flexible, since it is not limited to a specific surface (Figure S6 (Supporting Information) shows thermal gradients on a gold surface) or a specific heat source, as we used different laser sources (Figures S2, S4, and S5: Supporting Information). In addition, other materials, for example different metals or polymers may be used as temperature sensors to access an even broader temperature range.

Furthermore, after a heat source is thoroughly characterized, complex or even unknown mixtures of polymers (e.g., amino acids or other sensitive chemicals) can be screened for their critical temperature, inducing a phase change. This knowledge is particularly important for laser-induced forward transfer applications, where sensitive materials are processed.

The precision of our approach is defined by the optical resolution of the employed microscope. The alkanes or other thermal sensor materials have to be casted onto the substrate of interest and have to be chosen according to the expected temperature range. Besides these limitations, our method is cheap, easily accessible, and flexible.

In summary, by utilizing an ultrathin coating with a library of easy-to-use and inert materials, we can map short-lived temperature gradient on the micrometer scale on any surface with a cheap optical microscopy setup. This approach should also be applicable for a wide range of heat sources, such as hot needles, electric sparks, probing with an AFM tip, nano and micro-sized heating elements, or electronic devices.

4. Experimental Section

Reflection Optical Microscopy Setup and Lasing System: Figure 1 shows the experimental setup to determine on-line and locally (within lateral optical resolution) the (time-dependent) laser-induced changes in the sample and visualize the perimeter of melting and evaporation of the target material, due to the laser-induced heat in the substrate. A 405 nm continuous wave laser beam was focused in the polyimide film. The laser was used to irradiate the sample for different times (up to 100 ms) with different powers between 10 and 100 mW. The sample was imaged from the top in reflection mode (microscope head: Axio Scope.A1 Vario, ZEISS; camera Mikrotron GmbH; illumination: 6 W, λ = 445 nm, LDM-445-6000, LASERTACK, de-speckled by a rotational diffusor).

With the applied optics (objective, Olympus SLMPLN50x, numerical aperture = 0.35) nominally, a sample area of ≈0.49 µm × 0.49 µm was imaged on a single camera pixel. The setup enables the quasi-stationary, momentary imaging of the rupturing film. The high frame rate camera enabled a dynamic visualization of the melting of the films. A short exposure time of ≈100 µs avoided jitter.

Vertical Scanning Interferometry: High magnification (100x Nikon CF IC Epi Plan DI – Mirau) vertical scanning interferometer was performed with a smartWLI compact (Gesellschaft für Bild- und Signalverarbeitung (GBS) mbH, Illmenau, Germany) and the images were stitched together via Software.

Alkane and Polymer Films: Films are created via spin casting (spin coating) onto the planar interface on the polyimide or gold films. The coating parameters were chosen according to reference[37,38] to achieve typical film thicknesses of 10–300 nm. The alkanes were dissolved in high purity toluene (C_7H_8 Chromasolv Plus for HPLC, 99.9+ %). An excess volume (≈1 ml) was then spin cast at 50 rps onto the planar support until they were completely dry. The different initial solute concentrations can be found in the Supplementary Table S1. The polymer films were prepared as follows: 27 mg SLEC PLT 7552 (Sekisui Chemical GmbH, Germany) were dissolved in 450 µL dichloromethane (DCM) and 3 mg of N-[(9H-fluoren-9-ylmethoxy)carbonyl] (Fmoc) protected and pentafluorophenyl ester (OPfp)-activated l-amino acid in 50 µL *N,N*-dimethylformamide (DMF) were added. The mixture was spin-coated (spin casted) at 80 rps onto the polyimide film.

For the polyimide films, commercially available Kapton HN 100 tape (DuPont, USA; cmc Klebetechnik GmbH, Germany; thickness of polyimide layer ≈25 µm, thickness of glue layer ≈45 µm) was laminated onto typical 1 mm microscopy glass slides. The gold films were prepared via PVD at thicknesses of 20 and 50 nm.

Supporting Information

Supporting Information is available from the Wiley Online Library or from the author.

Conflict of Interest

The authors declare no conflict of interest.

[1] Y. Y. Liu, Y. Y. Zhu, Y. Cui, *Nat. Energy* **2019**, 4, 540.

[2] M. Seifrid, M. J. Ford, M. Q. Li, K. M. Koh, P. Trefonas, G. C. Bazan, *Adv. Mater.* **2017**, 29, 1605511.

[3] Y. H. Li, J. Chen, Y. F. Xing, J. H. Song, *Sci. Rep.* **2017**, 7, 6638.

[4] J. Dutta Majumdar, I. Manna, *Int. Mater. Rev.* **2011**, 56, 341.

[5] T. Sakimoto, M. I. Rosenblatt, D. T. Azar, *Lancet* **2006**, 367, 1432.

[6] D. B. Chrisey, *Science* **2000**, 289, 879.

[7] C. B. Arnold, A. Piqué, *MRS Bull.* **2007**, 32, 9.

[8] D. Zhang, B. Gökce, S. Barcikowski, *Chem. Rev.* **2017**, 117, 3990.

[9] U. Zywietz, A. B. Evlyukhin, C. Reinhardt, B. N. Chichkov, *Nat. Commun.* **2014**, 5, 3402.

[10] M. F. El-Kady, V. Strong, S. Dubin, R. B. Kaner, *Science* **2012**, 335, 1326.

[11] V. Strauss, K. Marsh, M. D. Kowal, M. El-Kady, R. B. Kaner, *Adv. Mater.* **2018**, 30, 1704449.

[12] P. Serra, A. Pique, *Adv. Mater. Technol.* **2019**, 4, 1800099.

[13] P. Serra, M. Colina, J. M. Fernández-Pradas, L. Sevilla, J. L. Morenza, *Appl. Phys. Lett.* **2004**, 85, 1639.

[14] P. Serra, J. M. Fernandez-Pradas, M. Colina, M. Duocastella, J. Dominguez, J. L. Morenza, *J. Laser Micro/Nanoeng.* **2006**, 1, 236.

[15] S. Eickelmann, A. Tsouka, J. Heidepriem, G. Paris, J. Zhang, V. Molinari, M. Mende, F. F. Loeffler, *Adv. Mater. Technol.* **2019**, 4, 1970062.

[16] D. S. Mattes, B. Streit, D. R. Bhandari, J. Greifenstein, T. C. Foertsch, S. W. Munch, B. Ridder, V. B.-K. C, A. Nesterov-Mueller, B. Spengler, U. Schepers, S. Brase, F. F. Loeffler, F. Breitling, *Macromol. Rapid Commun.* **2019**, 40, 1800533.

[17] F. F. Loeffler, T. C. Foertsch, R. Popov, D. S. Mattes, M. Schlageter, M. Sedlmayr, B. Ridder, F. X. Dang, C. von Bojnicic-Kninski, L. K. Weber, A. Fischer, J. Greifenstein, V. Bykovskaya, I. Buliev, F. R. Bischoff, L. Hahn, M. A. Meier, S. Brase, A. K. Powell, T. S. Balaban, F. Breitling, A. Nesterov-Mueller, *Nat. Commun.* **2016**, 7, 11844.

[18] G. Paris, A. Klinkusch, J. Heidepriem, A. Tsouka, J. Zhang, M. Mende, D. S. Mattes, D. Mager, H. Riegler, S Eickelmann, F. F. Loeffler, *Appl. Surf. Sci.* **2020**, 508, 144973.

[19] T. Bai, N. Gu, *Small* **2016**, 12, 4590.

[20] J. Christofferson, K. Maize, Y. Ezzahri, J. Shabani, X. Wang, A. Shakouri, in *2007 Int. Conf. on Thermal Issues in Emerging Technologies: Theory and Application*, IEEE, Piscataway, NJ **2007**, pp. 3–9.

[21] C. Cardenas, D. Fabris, S. Tokairin, F. Madriz, C. Y. Yang, *J. Heat Transfer* **2012**, 134, 111401.

[22] D. Kendig, G. Hohensee, E. Pek, W. Kuang, K. Yazawa, A. Shakouri, in *2017 16th IEEE Intersociety Conf. on Thermal and Thermomechanical Phenomena in Electronic Systems (ITherm)*, IEEE, Piscataway, NJ **2017**, pp. 23–29.

[23] J. Zhu, X. Wu, D. M. Lattery, W. Zheng, X. Wang, *Nanoscale Microscale Thermophys. Eng.* **2017**, 21, 177.

[24] X. Huo, H. Liu, Y. Liang, M. Fu, W. Sun, Q. Chen, S. Xu, *Small* **2014**, 10, 3869.

[25] A. Csendes, V. Szekely, M. Rencz, *Microelectron. Eng.* **1996**, 31, 281.

[26] C. E. Stephens, F. N. Sinnadurai, *J. Phys. E: Sci. Instrum.* **1974**, 7, 641.

[27] J. Xiong, M. Zhao, X. Han, Z. Cao, X. Wei, Y. Chen, C. Duan, M. Yin, *Sci. Rep.* **2017**, 7, 41311.

[28] P. Wang, H. Xia, Q. Li, F. Wang, L. Zhang, T. Li, P. Martyniuk, A. Rogalski, W. Hu, *Small* **2019**, 15, 1904396.

[29] S. Eickelmann, J. Danglad-Flores, G. Chen, M. S. Miettinen, H. Riegler, *Langmuir* **2018**, 34, 11364.

[30] H. Riegler, R. Köhler, *Nat. Phys.* **2007**, 3, 890.

[31] A. Ksiazczak, K. Moorthi, I. Nagata, *Fluid Phase Equilib.* **1994**, 95, 15.

[32] P. Lazar, H. Riegler, *Phys. Rev. Lett.* **2005**, 95, 136103.

[33] T. Pfohl, D. Beaglehole, H. Riegler, *Chem. Phys. Lett.* **1996**, 260, 82.

[34] C. Jin, H. Riegler, *J. Phys. Chem. C* **2016**, *120*, 16815.

[35] H. Bloom, F. G. Davis, D. W. James, *Trans. Faraday Soc.* **1960**, *56*, 1179.

[36] V. Stadler, T. Felgenhauer, M. Beyer, S. Fernandez, K. Leibe, S. Guttler, M. Groning, K. Konig, G. Torralba, M. Hausmann, V. Lindenstruth, A. Nesterov, I. Block, R. Pipkorn, A. Poustka, F. R. Bischoff, F. Breitling, *Angew. Chem., Int. Ed.* **2008**, *47*, 7132.

[37] J. Danglad-Flores, K. Eftekhari, A. G. Skirtach, H. Riegler, *Langmuir* **2019**, *35*, 3404.

[38] S. Eickelmann, H. Riegler, *J. Colloid Interface Sci.* **2018**, *528*, 63.